

We are IntechOpen, the world's leading publisher of Open Access books Built by scientists, for scientists

6,900

Open access books available

186,000

International authors and editors

200M

Downloads

Our authors are among the

154

Countries delivered to

TOP 1%

most cited scientists

12.2%

Contributors from top 500 universities



WEB OF SCIENCE™

Selection of our books indexed in the Book Citation Index
in Web of Science™ Core Collection (BKCI)

Interested in publishing with us?
Contact book.department@intechopen.com

Numbers displayed above are based on latest data collected.
For more information visit www.intechopen.com



Modeling and Simulation of the Variable Speed Wind Turbine Based on a Doubly Fed Induction Generator

Imane Idrissi, Houcine Chafouk, Rachid El Bachtiri and Maha Khanfara

Abstract

This chapter presents the modeling and simulation results of variable speed wind turbine driven by doubly fed induction generator (DFIG). The feeding of the generator is ensured through its stator directly connected to the electrical grid and by its rotor connected to the grid through two power converters, which are controlled by the pulse width modulation (PWM) technique. This configuration is the most used in the wind power generation systems. For the variable speed operation of the studied system, the maximum power point tracking strategy is applied for the turbine, and the stator flux-oriented vector control is used for the generator. The MATLAB/Simulink software is used for the system modeling and simulation. For the wind velocity model, a random wind profile is simulated, and the turbine and the generator parameters are extracted from an existing wind turbine system in the literature. The obtained results are addressed in this chapter.

Keywords: wind turbine, variable speed operation, DFIG, PWM, MATLAB/Simulink, MPPT

1. Introduction

With the global warming issues and the climate changes, there is a serious need for the use of the renewable energy resources in the electricity generation industry. Currently, the wind represents one of the most important renewable energy resources, used for generating electrical energy in the world. In terms of the total installed wind capacity, it becomes up to 539 GW across the globe in 2017 [1]. The rapid rate of the wind energy industry growth is caused by the cost-effectiveness of electricity production from wind farms, compared to electricity production cost from fossil fuel energy [2], the stability of electricity cost [3], the short commissioning time of wind farms [4], and the ingenuity of skillful engineers.

According to a wind market survey, the doubly fed induction generator (DFIG) is the most popular generator used in the speed variable wind turbines (SVWT) [5]. It is a wound rotor asynchronous machine which has the stator windings directly

connected to the electrical grid, and its rotor is linked to the constant frequency grid by means of two bidirectional power converters.

This configuration, known as “Scherbius structure” and shown in **Figure 1**, has several advantages of controlling independently active and reactive power [6, 7]. Moreover, the power converters used are sized to transfer only a fraction, equal to at most 30% of the turbine rated power [8, 9], which results in small-size, low-cost, less acoustic noise and reduced loss rate in the power converters [10]. Moreover, The DFIG-based wind turbine allows the rotor speed to be varied with the wind speed, and the speed variation range is around $\pm 30\%$ around the synchronism speed [11]. As a result, the wind generation system could operate in hyposynchronous and hypersynchronous mode, which would extract the maximum aerodynamic power for each wind speed value.

In order to design fault diagnosis and control approaches based on models for wind turbines, the development of a mathematical model, which represents as much details as technically possible and gives an accurate idea of the dynamic behavior of the system, seems to be an important step. For several purposes, different wind turbine models have been developed. In literature, we find for wind systems the aerodynamic model, which aims to verify and optimize the blade design, depending on predefined specifications, while the mechanical model is used by engineers for establishing a safe and economical dimensioning of the whole wind turbine system. Moreover, the economic model is used in the case of manufacturing and installing wind turbines with the purpose to evaluate the cost-effectiveness. In addition, there are models which predict the weather conditions and the power output of wind farms. Furthermore, there are models, which have the objective of evaluating the impact of wind turbines on the environment such as the evaluation of noise produced by the wind turbine operation. Finally, the general-purpose models concerned with the electrical properties of wind turbines are widely used.

The speed variable wind turbine (SVWT) model, developed and simulated in this work, is concerned with providing time simulation signals that can be exploited for designing fault diagnosis approaches based on models; the software tool used for simulation is the MATLAB/Simulink environment. In [12], a wind turbine model of a fixed-speed, stall-regulated system has been developed with the aim of measuring and evaluating the power quality impact of wind turbines on the grid. In addition, a model for a wind turbine generation system based on a DFIG, including the mechanical dynamics, the wind turbine electrical system, the converter, and the electrical grid has been presented in [13]. Luis et al. [14] presented the most commonly used wind turbine model meeting objectives as production energy, safety of turbine, grid connection, and others. Moreover, in [15], the detailed

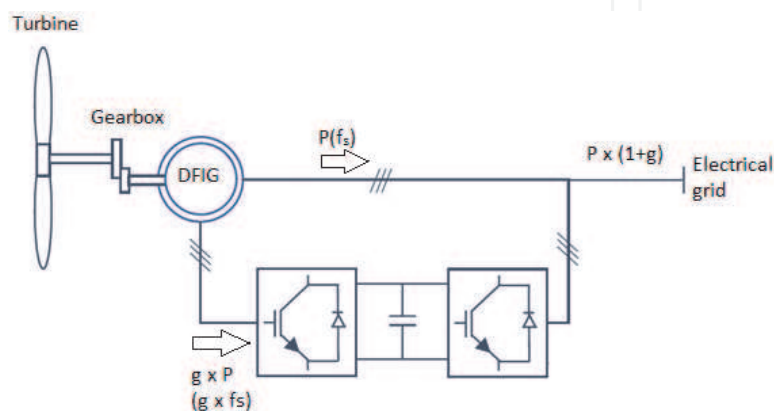


Figure 1.
Architecture Scherbius of DFIG-based wind turbine.

mechanical structural modeling of the wind turbine connected to the grid and based on DFIG has been developed, and it has been validated using NREL's simulation tool, FAST v7; for analysis of the dynamic behavior of the wind power plant with DFIG under the grid fault conditions, modeling of the whole system has been established in [16]. Furthermore, with the use of an electromagnetic transient simulation software, the wind turbine driven by DFIG model is elaborated in [17].

The organization of this chapter is as follows: the wind turbine structure is described in Section 2; the wind modeling turbine is presented in Section 3. In Section 4, the simulation results in MATLAB/Simulink environment are shown. Finally, the conclusion is presented in Section 5.

2. The wind turbine structure

The wind turbine is a complex system containing different components, which involved different domains: electrical, mechanical, and electronic areas and others. The complete model of the studied wind turbine system is represented by a set of blocks each representing a functional entity of the system. The general structure of a wind system is given by **Figure 2**.

As it is shown in the **Figure 2**, the wind velocity and the fixed-pitch angle represent the input of the wind turbine system. The aerodynamic conversion entity is formed of three blades which capture and convert the kinetic energy of the wind into mechanical energy, recovered on the slow rotating shaft. Then, the gearbox device increases the turbine low speed and makes it suitable with the generator rotational speed, which is about 1500 rpm. The generator receives mechanical energy and transforms it into electrical energy. The two power converters used are insulated gate bipolar transistor (IGBT) type and controlled by pulse width modulation (PWM) technique; they allow the independent control of the active and reactive powers and also the transfer of the slip power in two directions: from the generator to the network and from the network to the generator.

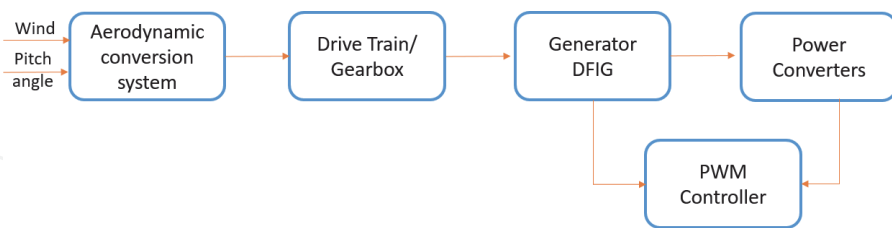


Figure 2.
Wind turbine system structure.

3. The wind turbine modeling

In this section, the mathematical model of each wind turbine block is presented.

3.1 Wind speed model

The wind resource is an important element in a wind energy system, and it represents a determining factor in the calculation of electricity production because, under optimal conditions, the power captured by the wind turbine is a cubic

function of the wind speed. The wind is a moving air mass, and the wind kinetic energy is given by:

$$E = \frac{1}{2} \cdot m \cdot v^2 \quad (1)$$

where m is the moving air mass [g] and v is the air moving speed [m/s].

The wind power during is expressed as:

$$P_{wind} = \frac{E}{\Delta t} \quad (2)$$

The wind speed v is generally represented by a scalar function evolving over time, given by $V = f(t)$. It can also be divided into two components: a slowly varying part denoted as V_0 and a random varying part denoted as V_t ; it represents the wind fluctuations. Therefore, the wind velocity can be written as:

$$V(t) = V_0 + V_t(t) \quad (3)$$

To mathematically model the wind speed profile, the literature offers three techniques:

- The first method is white noise filtering technique, in which the turbulence impact is corrected by the use of a low-pass filter having the following transfer function [18]:

$$F(s) = \frac{1}{1 + \tau \cdot s} \quad (4)$$

where τ is the filter time constant. It depends on the rotor diameter and the wind turbulence intensity and the average wind speed. **Figure 3** shows the method of reconstruction of the wind profile using this technique.

- The second method of generating the wind speed profile is that which describes wind variations using the spectral density established by meteorologist I. Van der Hoven. In this model, the turbulence part is considered as a stationary random process, and therefore it does not depend on

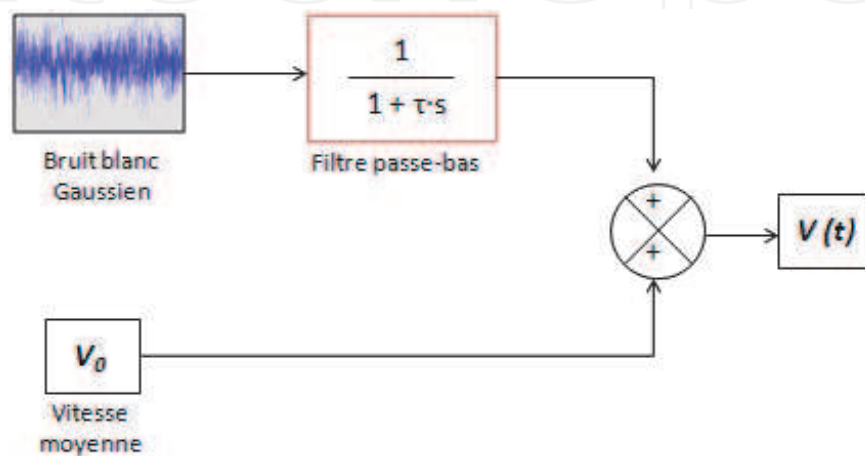


Figure 3.
Wind profile construction scheme by white noise filtering.

the variation of the mean wind speed [19, 20]. The variation of the wind speed $v(t)$ is thus written in the form of the harmonic sum:

$$V_v(t) = A + \sum_{i=1}^n a_k \cdot \sin(\omega_k \cdot t) \quad (5)$$

where A is the wind speed average value; a_k is the amplitude of k -order harmonic; ω_k is the pulsation of k -order harmonic; and i is the last harmonic rank retained in the wind profile calculation.

- The third method is the Weibull distribution in which a given site wind potential is obtained by measuring the average wind speed in regular time intervals. Then, the data obtained are then divided into numbers by wind speed classes using histogram [21]. The wind profile over a desired time period, respecting the Weibull distribution, is given by:

$$V_v(t) = (1 + \xi_v(t) - \xi_v) \cdot V_v \quad (6)$$

where V_v is the wind speed average value and ξ_v is the disturbance mean value expressed by:

$$\xi_v(t) = \left(-\frac{\ln(\text{rand}(t))}{c_v} \right)^{\frac{1}{k_v}} \quad (7)$$

where $\text{rand}(t)$ is a function generating, in a uniform distribution, random numbers between 0 and 1 and (C_v, k_v) is a parameter pair, determined by analysis of the wind class histogram. C_v is a scale factor generally greater than 5. The shape factor k_v is greater than 3 if the histogram shape is like that of a normal distribution, characterized by an uniform distribution around a mean value.

In this work, we adopted the second method to generate the random profile of the wind speed applied in the studied wind system input.

3.2 Aerodynamic conversion model

The aerodynamic conversion system is the wind turbine part, which is facing the wind; it generally comprises three blades of length R . Three-bladed wind turbines are much more common than two-bladed wind turbines. The turbine captures the kinetic energy of the wind and transforms it into mechanical energy recovered on the slow rotating shaft.

The kinetic power of the wind is given by:

$$P_{wind} = \frac{\rho \cdot S \cdot v_{wind}^3}{2} \quad (8)$$

The aerodynamic power is expressed as follows:

$$P_{aero} = C_p(\lambda, \beta) \cdot P_{wind} = C_p(\lambda, \beta) \cdot \frac{\rho \cdot S \cdot v_{wind}^3}{2} \quad (9)$$

The aerodynamic torque T_{aer} is given by the following expression:

$$T_{aer} = \frac{P_{aero}}{\Omega_t} = \frac{1}{2 \cdot \Omega_t} \cdot C_p(\lambda, \beta) \cdot \rho \cdot S \cdot v_{wind}^3 \quad (10)$$

where Ω_t is the turbine speed [rad/s], ρ is the air density, $\rho = 1.225 \text{ kg/m}^3$, $S = \pi R_2^2$ is the rotor surface [m^2], R is the blade length [m], and v_{wind} is the wind speed upstream of the wind turbine rotor [m/s]. λ is the speed ratio. It is a unitless parameter, related to the design of each wind turbine, and it represents the ratio between the speed of the blade's end and that of the wind at the rotor axis or also called hub. λ is expressed as follows:

$$\lambda = \frac{\Omega_t \cdot R}{v} \quad (11)$$

This parameter depends on the blade number of the wind turbine. If the blade number is reduced, the rotor speed is high, and a maximum of power is extracted from the wind. In the case of multiblade wind turbines (Western Wind Turbines), the speed ratio is equal to 1; for wind turbines with a single blade, λ is about 11. The three-bladed wind turbines, as in our study, have a speed ratio of 6 to 7. The speed ratio of Savonius wind turbines is less than 1 [22].

C_p is the power coefficient or aerodynamic transfer efficiency that varies with the wind speed. This coefficient has no unit, and it depends mainly on the blade aerodynamics, the speed ratio λ , and the blade orientation angle β . Betz has determined a theoretical maximum limit of the power coefficient $C_{p\text{max}} = 16/27 \sim 0.59$. Taking into account losses, wind turbines never operate at this maximum limit, and the best-performing wind turbines have a C_p between 0.35 and 0.45. C_p is specific to each wind turbine, and its expression is given by the wind turbine manufacturer or using nonlinear formulas. To calculate the coefficient C_p , different numerical approximations have been proposed in the literature. The C_p expressions frequently encountered in the literature are presented in **Table 1**.

Since we had as an objective the modeling and simulation of a three-bladed wind turbine with a nominal power of 3 kW; the parameters of both: the wind turbine and the generator have been used from [30]. For this reason, the analytical expression of the power coefficient C_p is given by:

$$C_p = 6 \cdot 10^{-7} \cdot \lambda^5 + 10^{-5} \cdot \lambda^4 - 65 \cdot 10^{-5} \cdot \lambda^3 + 2 \cdot 10^{-5} \cdot \lambda^2 + 76 \cdot 10^{-3} \cdot \lambda + 0.007 \quad (12)$$

This coefficient has a maximum value equal to 0,35 ($C_{p\text{max}} = 0,35$) and an optimal value of relative speed equal to 7 ($\lambda = 7$).

The block diagram presenting the aerodynamic part is shown in **Figure 4**.

3.3 Gearbox model

The mechanical part of the wind turbine consists of the turbine shaft rotating slowly at speed Ω_t , the gearbox having the multiplication gain G and driving the generator at a speed Ω_g , by means of a fast secondary shaft.

The gearbox is a device that allows to multiply the turbine speed of Ω_t by a multiplication gain G to make it adapt to the rapid speed of the generator Ω_g . This device is considered ideal, because the gearbox elasticity, friction, and energy losses are considered negligible. The two equations mathematically modeling the operation of this device are given as follows:

$$\begin{cases} T_g = \frac{T_{\text{aer}}}{G} \\ \Omega_t = \frac{\Omega_g}{G} \end{cases} \quad (13)$$

Power coefficient type, Cp	Formula
Exponential	$0.22 \cdot \left[\frac{116}{\lambda_i} - 0.4 \cdot \beta - 5 \right] \cdot e^{\frac{12.5}{\lambda_i}} \text{avec } \frac{1}{\lambda_i} = \frac{1}{\lambda + 0.08 \cdot \beta} - \frac{0.035}{\beta^3 + 1}$ [23]
	$0.5 \cdot \left[\frac{116}{\lambda_i} - 0.4 \cdot \beta - 5 \right] \cdot e^{-\frac{21}{\lambda_i}} + 0.068 \cdot \lambda$ [8, 24, 25] Avec: $\frac{1}{\lambda_i} = \frac{1}{\lambda + 0.08 \cdot \beta} - \frac{0.035}{\beta^3 + 1}$
	$0.5176 \cdot \left[\frac{116}{\lambda_i} - 0.4 \cdot \beta - 5 \right] \cdot e^{-\frac{21}{\lambda_i}} + 0.0068 \cdot \lambda$ [26] Avec: $\frac{1}{\lambda_i} = \frac{1}{\lambda + 0.08 \cdot \beta} - \frac{0.035}{\beta^3 + 1}$
	$0.5109 \cdot \left[\frac{116}{\lambda_i} - 0.4 \cdot \beta - 5 \right] \cdot e^{-\frac{21}{\lambda_i}} + 0.0068 \cdot \lambda$ [27] Avec: $\frac{1}{\lambda_i} = \frac{1}{\lambda + 0.08 \cdot \beta} - \frac{0.035}{\beta^3 + 1}$
	$0.44 \cdot \left[\frac{125}{\lambda_i} - 6.94 \right] \cdot e^{-\frac{16.5}{\lambda_i}}$ [21] Avec: $\lambda_i = \frac{1}{\frac{1}{\lambda} + 0.002}$
Sinusoidal	$0.5 - 0.167 \cdot (\beta - 2) \cdot \sin \left[\frac{\pi \cdot (\lambda - 3)}{18.9 - 0.3 \cdot (\beta - 2)} \right] - 0.00184 \cdot (\lambda - 3) \cdot (\beta - 2)$ [28]
	$0.3 - 0.00167 \cdot (\beta - 2) \cdot \sin \left[\frac{\pi \cdot (\lambda + 0.1)}{10 - 0.3 \cdot (\beta - 2)} \right] - 0.00184 \cdot (\lambda - 3) \cdot \beta$ [29]
Polynomial	$6 \cdot 10^{-7} \cdot \lambda^5 + 10^{-5} \cdot \lambda^4 - 65 \cdot 10^{-5} \cdot \lambda^3 + 2 \cdot 10^{-5} \cdot \lambda^2 + 76 \cdot 10^{-3} \cdot \lambda + 0.007$ [30]
	$79.5633 \cdot 10^{-5} \cdot \lambda^{-5} - 17.375 \cdot 10^{-4} \cdot \lambda^4 + 9.86 \cdot 10^{-3} \cdot \lambda^3 - 9.4 \cdot 10^{-3} \cdot \lambda^2 + 6.38 \cdot 10^{-2} \cdot \lambda + 0.001$ [31]

Table 1.
Different numerical formulas of the power coefficient Cp.

where T_g is torque on the generator shaft ($N \cdot m$), T_{aer} is the aerodynamic torque of the wind turbine ($N \cdot m$), Ω_g is the speed generator shaft ($rad \cdot s^{-1}$), Ω_t is the turbine speed shaft ($rad \cdot s^{-1}$), and G is the multiplication gain; it is given by $G = N1/N2$.

Figure 5 shows the gearbox model for determining the multiplication gain G , and **Figure 6** shows the gearbox block diagram.

The total inertia J consists of the turbine inertia J_t and the generator inertia J_g ; it can be written according to the following equation [28]:

$$J = \frac{J_t}{G^2} + J_g \quad (14)$$

The total viscous friction coefficient f_v consists of the generator friction coefficient f_g and the turbine friction coefficient f_t . The coefficient f_v can be expressed as follows:

$$f_v = \frac{f_t}{G^2} + f_g \quad (15)$$

Therefore, the mechanical part can be modeled according to the diagram shown in **Figure 7**.

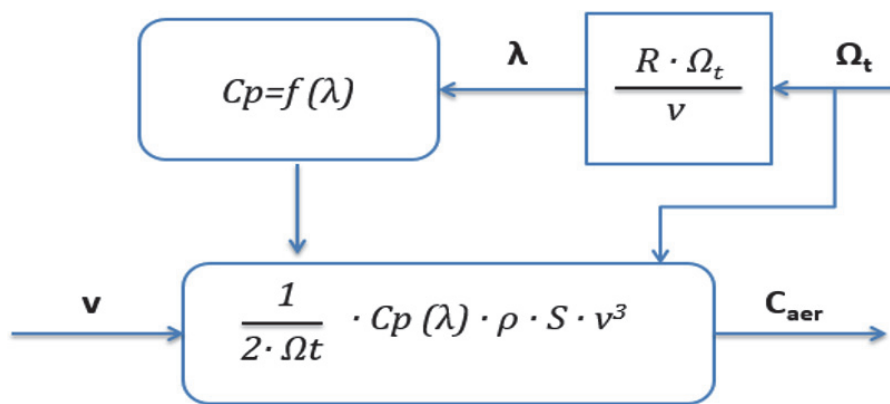


Figure 4.
Block diagram of the aerodynamic part.

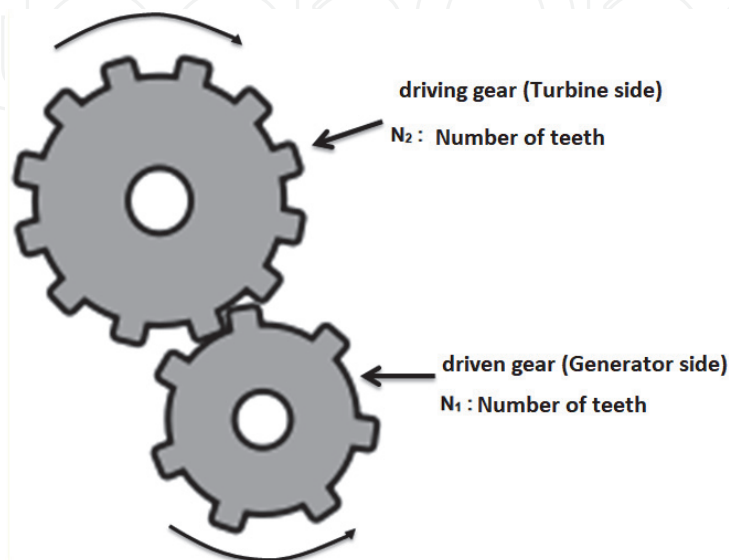


Figure 5.
The gearbox model.

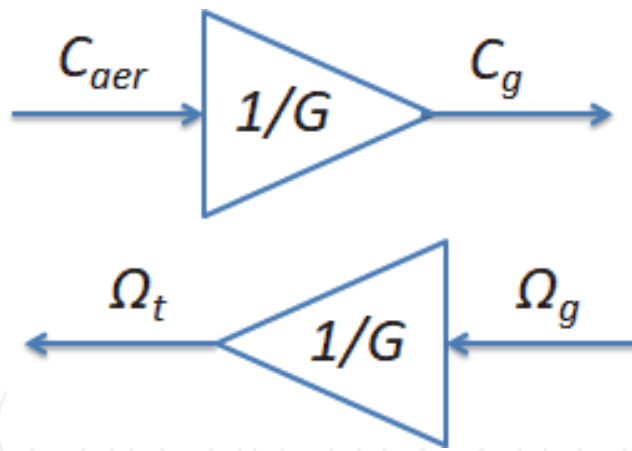


Figure 6.
 Block diagram of the gearbox.

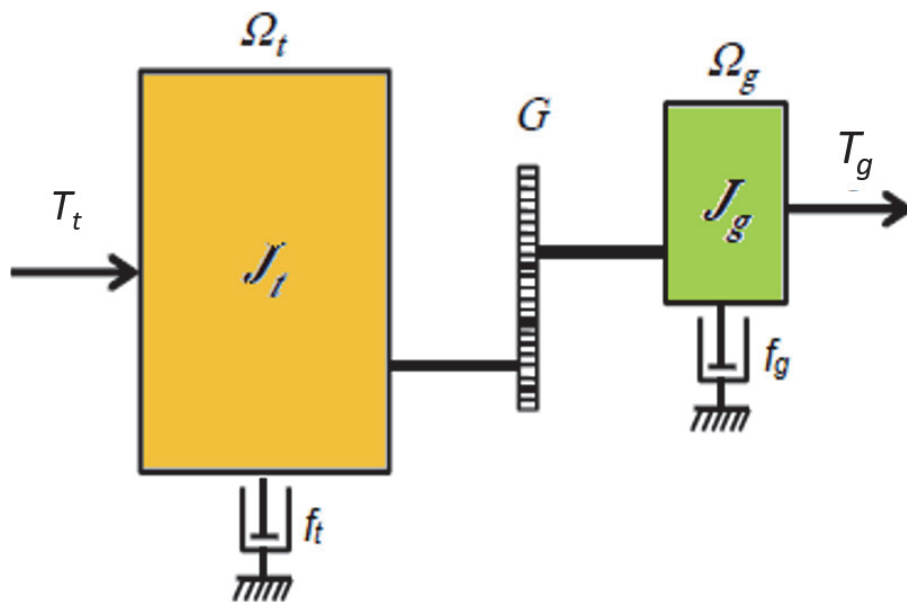


Figure 7.
 The several coefficients of the wind turbine mechanical part.

The generator speed Ω_g depends on the total mechanical torque T_{mec} . This torque is the result of the electromagnetic torque of the generator T_{em} , the viscous friction torque T_v , and the torque applied on the generator shaft T_g .

$$T_{mec} = J \cdot \frac{d\Omega_g}{dt} \quad (16)$$

$$T_{mec} = T_g - T_{em} - T_v \quad (17)$$

$$T_v = f \cdot \Omega_g \quad (18)$$

Therefore, from these previously established equations, the differential equation of the mechanical system dynamics is expressed by:

$$J \cdot \frac{d\Omega_g}{dt} = T_g - T_{em} - T_{vis} \quad (19)$$

The block diagram of the wind turbine mechanical part is presented in **Figure 8**. The diagram block of the whole wind turbine system is given in **Figure 9**.

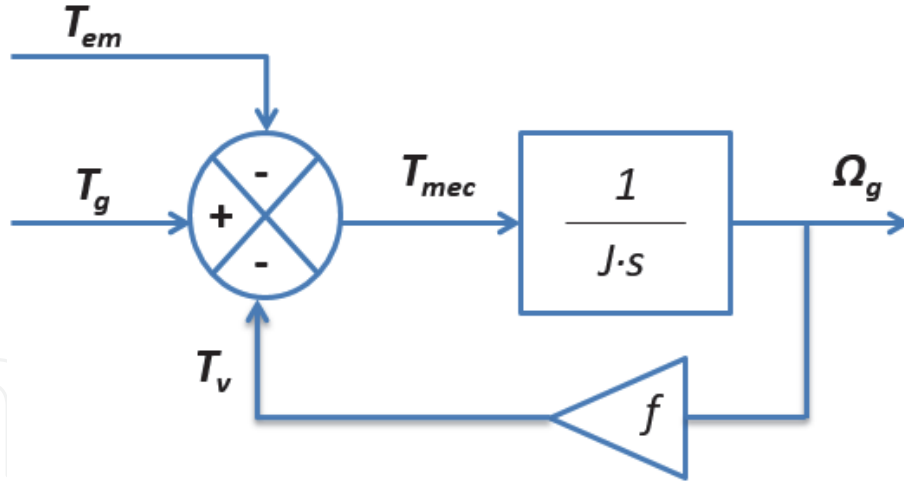


Figure 8.
Block diagram of the wind turbine mechanical part.

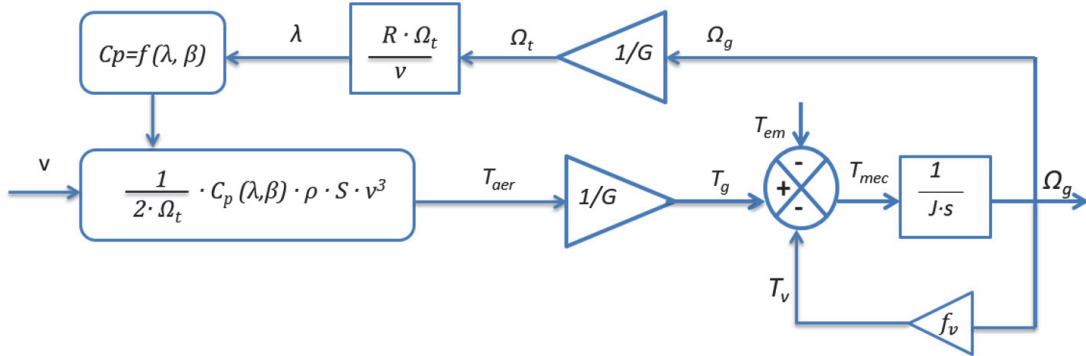


Figure 9.
Block diagram of the whole wind turbine system.

In order to continuously reach the maximum power point provided by a wind turbine, operating over a wide range of wind speed, the maximum power point tracking (MPPT) control technique is used. In this chapter, the MPPT control without controlling the mechanical speed is presented [32]. This control strategy is based on the assumption that the wind speed little varies in steady state compared to the electrical constants of the wind turbine system. Therefore, at the maximum power point, the relative speed λ is equal to its optimum value λ_{opt} , and the power coefficient C_p is equal to its maximum value C_{p-max} , while the reference electromagnetic torque C_{em}^* is given by:

$$C_{em}^* = \frac{C_{aer-est}}{G} \quad (20)$$

$$C_{em}^* = C_{p-max} \cdot \frac{\rho \cdot \pi \cdot R^5 \cdot \Omega_g^2}{2 \cdot \lambda_{opt}^3 \cdot G^3} \quad (21)$$

For simplification, the parameter K is expressed as:

$$K = C_{p-max} \cdot \frac{\rho \cdot \pi \cdot R^5}{2 \cdot \lambda_{opt}^3 \cdot G^3} \quad (22)$$

Therefore:

$$C_{em}^* = K \cdot \Omega_g^2 \quad (23)$$

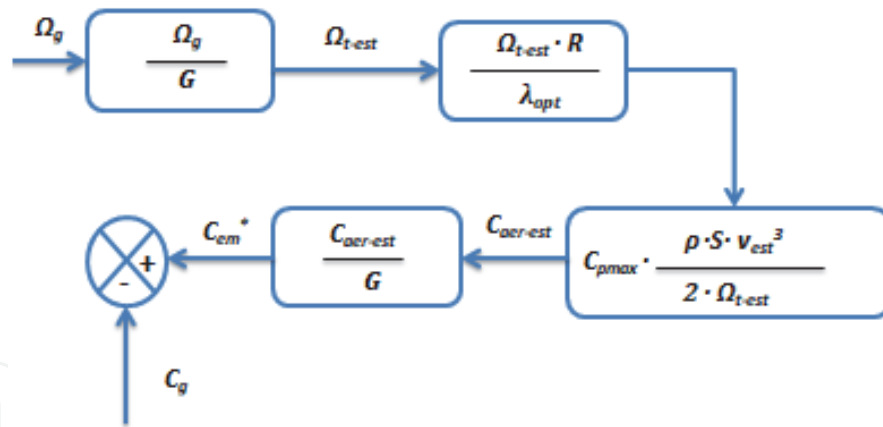


Figure 10.
 Block diagram of the MPPT control without mechanical speed.

The reference electromagnetic torque is proportional to the square of the generator speed Ω_g . The block diagram which presents the MPPT control strategy without the measurement of the generator speed is shown in **Figure 10**.

3.4 DFIG model

The doubly fed induction generator (DFIG) is a three-phase asynchronous machine, powered by two sources: by its stator and its rotor at the same time. Its main advantage is that it offers the possibility of controlling the power flows for the hypo- and hypersynchronous modes, either in the motor or generator operation. It also allows the variable speed operation of the system where it is integrated.

The DFIG model in the stationary reference frame, noted (α, β) , is given in the state representation [33] as follows:

$$\frac{d}{dt} \begin{bmatrix} i_{s\alpha} \\ i_{s\beta} \\ i_{r\alpha} \\ i_{r\beta} \end{bmatrix} = [A] \cdot \begin{bmatrix} i_{s\alpha} \\ i_{s\beta} \\ i_{r\alpha} \\ i_{r\beta} \end{bmatrix} + [B] \cdot \begin{bmatrix} v_{s\alpha} \\ v_{s\beta} \\ v_{r\alpha} \\ v_{r\beta} \end{bmatrix} \quad (24)$$

where $i_{s\alpha}$ and $i_{s\beta}$ are the stator currents in the stationary reference frame (α, β) ; $i_{r\alpha}$ and $i_{r\beta}$ are the rotor currents in the reference frame (α, β) ; $v_{s\alpha}$ and $v_{s\beta}$ are the stator stresses in the stationary reference frame (α, β) ; $v_{r\alpha}$ and $v_{r\beta}$ are the rotor voltages in the stationary reference frame (α, β) .

The matrices $A \in \mathbb{R}^{n \times n}$, $B \in \mathbb{R}^{n \times m}$, and $C \in \mathbb{R}^{p \times n}$ are, respectively, the state matrix, the input or control matrix, and the output or observation matrix. They are, respectively, given by:

$$A = \begin{bmatrix} \frac{-R_s}{\sigma \cdot L_s} & \left(\frac{(1-\sigma)}{\sigma} \cdot \omega + \omega_s \right) & \frac{M \cdot R_r}{\sigma \cdot L_s \cdot L_r} & \frac{M}{\sigma \cdot L_s} \cdot \omega \\ -\left(\frac{(1-\sigma)}{\sigma} \cdot \omega + \omega_s \right) & \frac{-R_s}{\sigma \cdot L_s} & -\frac{M}{\sigma \cdot L_s} \cdot \omega & \frac{M \cdot R_r}{\sigma \cdot L_s \cdot L_r} \\ \frac{M \cdot R_s}{\sigma \cdot L_s \cdot L_r} & -\frac{M}{\sigma \cdot L_r} \cdot \omega & \frac{-R_r}{\sigma \cdot L_r} & \left(\omega_s - \frac{\omega}{\sigma} \right) \\ \frac{M}{\sigma \cdot L_r} \cdot \omega & \frac{M \cdot R_s}{\sigma \cdot L_s \cdot L_r} & -\left(\omega_s - \frac{\omega}{\sigma} \right) & \frac{-R_r}{\sigma \cdot L_r} \end{bmatrix}$$

$$B = \begin{bmatrix} \frac{1}{\sigma \cdot L_s} & 0 & -\frac{M}{\sigma \cdot L_s \cdot L_r} & 0 \\ 0 & \frac{1}{\sigma \cdot L_s} & 0 & -\frac{M}{\sigma \cdot L_s \cdot L_r} \\ -\frac{M}{\sigma \cdot L_s \cdot L_r} & 0 & \frac{1}{\sigma \cdot L_r} & 0 \\ 0 & -\frac{M}{\sigma \cdot L_s \cdot L_r} & 0 & \frac{1}{\sigma \cdot L_r} \end{bmatrix}$$

$$C = \begin{bmatrix} 1 & 0 & 0 & 0 \\ 0 & 1 & 0 & 0 \\ 0 & 0 & 1 & 0 \\ 0 & 0 & 0 & 1 \end{bmatrix}$$

where R_s and L_s are, respectively, the single-phase resistance and the cyclic single-phase inductance of the stator winding; R_r and L_r are, respectively, the single-phase resistance and the cyclic single-phase inductance of the rotor winding; M is the mutual inductance between the stator phase and the rotor phase; $\sigma = 1 - \frac{M^2}{L_s \cdot L_r}$ is the leakage coefficient or the Blondel coefficient; ω_s is the synchronism angular speed [rad/s]; and ω is the mechanical angular speed [rad/s].

In order to generate the reference rotor voltages which will be the input of the machine side converter, the stator flux-oriented vector control is applied to DFIG system [34].

3.5 Power converter models

The power electronic converters used consist of a rectifier made using semi-conductors controlled at the opening and closing, and a three-phase voltage inverter consists of three reversible current switch arms, controlled at the opening and closing in the same time. Each arm consists of two switches, which contain each one insulated gate bipolar transistor (IGBT) and an antiparallel diode. The voltage capacitor DC allows the storage of the output rectifier energy. The passive filter type (L, R) is used to connect the inverter to the grid. Both converters used are controlled using pulse width modulation (PWM), and the power converter structure is given in **Figure 11**.

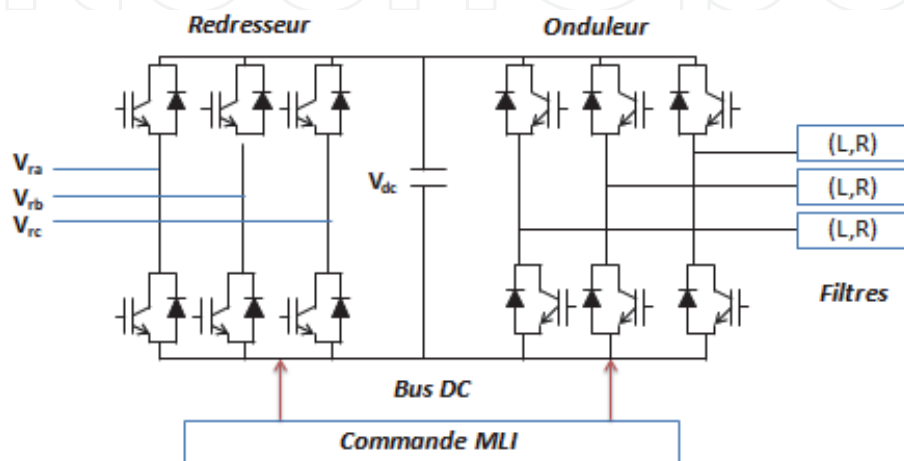


Figure 11. Structure of the power converters (IGBT).

The input voltages of single phases of the rotor side converter (RSC) are described as follows:

$$\begin{cases} V_{S_a} = \frac{2 \cdot S_a - S_b - S_c}{3} \cdot V_{dc} \\ V_{S_b} = \frac{2 \cdot S_b - S_a - S_c}{3} \cdot V_{dc} \\ V_{S_c} = \frac{2 \cdot S_c - S_a - S_b}{3} \cdot V_{dc} \end{cases} \quad (25)$$

where S_i represents the switch states, supposedly ideal to facilitate the rectifier modeling, defined by:

$$S_i = \begin{cases} 1, \bar{S}_i = 0 \\ 0, \bar{S}_i = 1 \end{cases}; i = a, b, c \quad (26)$$

The rotor voltage equations and the DC capacitor equation are given, respectively:

$$[V_{rabc}] = R_r \cdot [i_{rabc}] + L_r \cdot \frac{d}{dt} [i_{rabc}] + [V_{Sabc}] \quad (27)$$

$$C \cdot \frac{dV_{dc}}{dt} = (S_a \cdot i_{S_a} + S_b \cdot i_{S_b} + S_c \cdot i_{S_c}) - i_{dc} \quad (28)$$

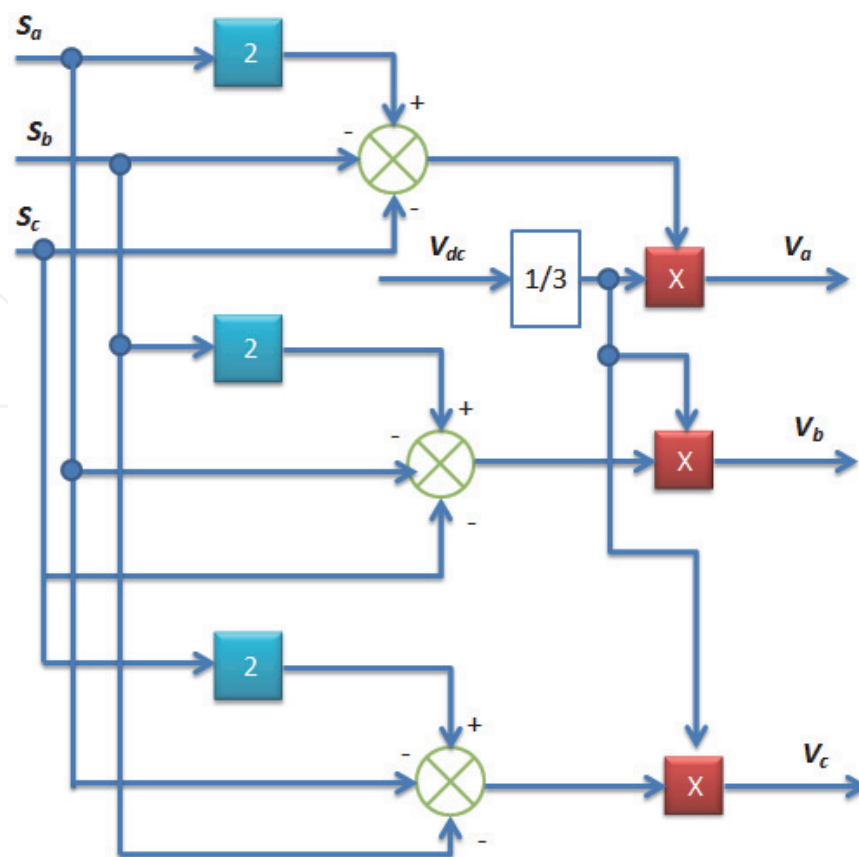


Figure 12.
 The block diagram of the RSC.

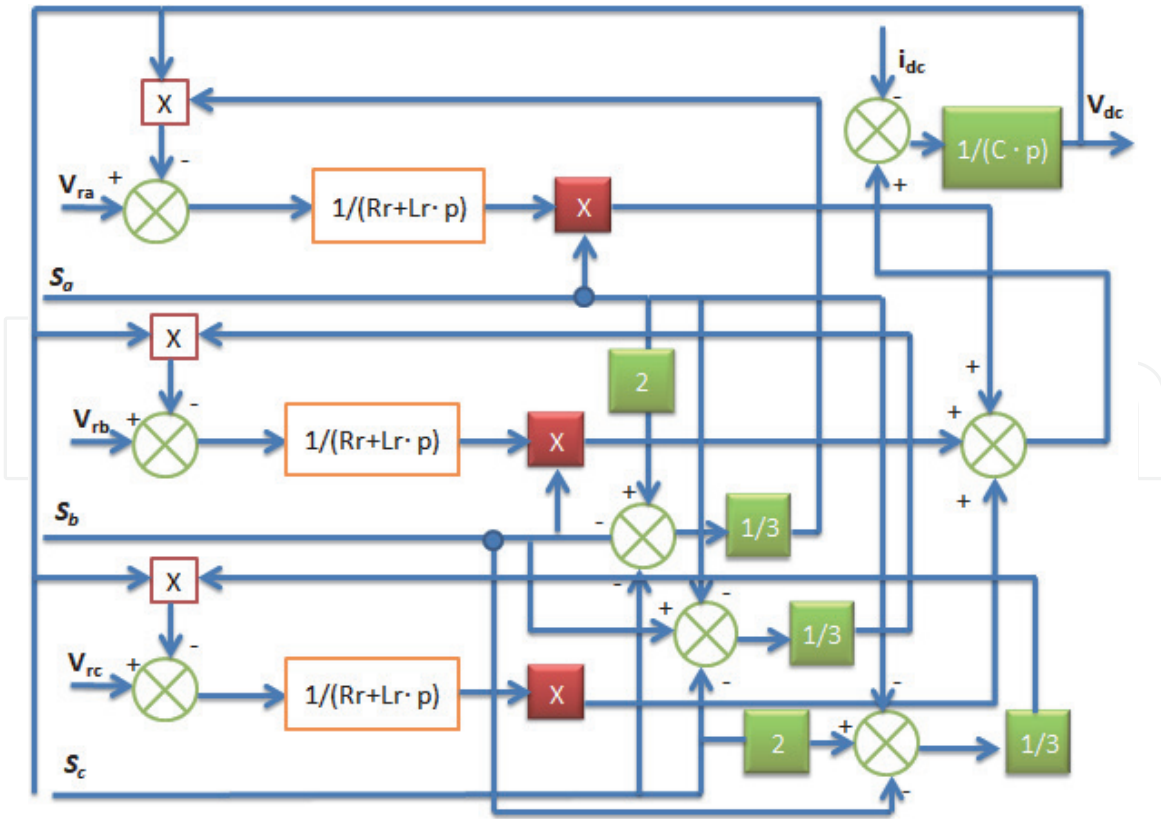


Figure 13.
The block diagram of the GSC.

where V_{rabc} is the three-phase rotor voltage of DFIG [V]; i_{rabc} is the three-phase rotor current of DFIG [A]; C is the capacitor constant [F]; V_{dc} is the DC bus voltage [V]; i_{dc} is the DC output current [A].

The block diagrams of the rotor side converter (RSC) and the grid side converter (GSC) are given, respectively, in **Figures 12 and 13**.

4. Simulation results

The variable speed wind turbine model based on DFIG with a power of 3 Kw has been developed and simulated using MATLAB/Simulink software. The

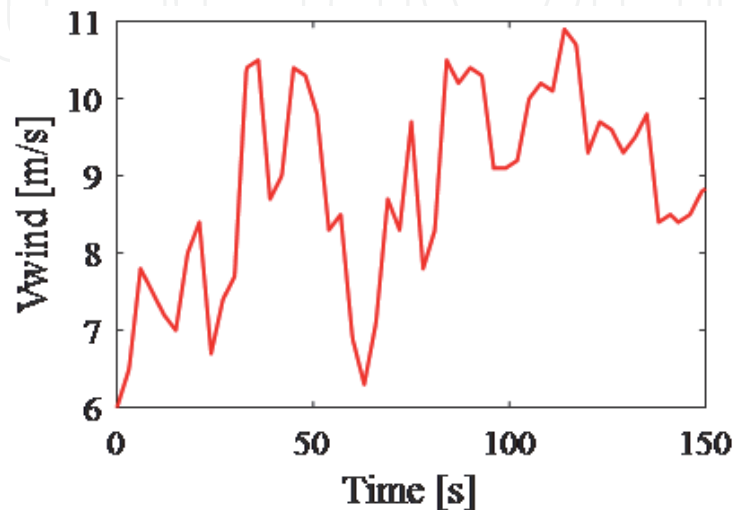


Figure 14.
Wind speed profile [m/s].

turbine and DFIG parameters are extracted from [30]. Some simulation results of the wind system modeled in this study are presented in the figures below.

Figure 14 shows the random wind speed profile applied to the turbine.

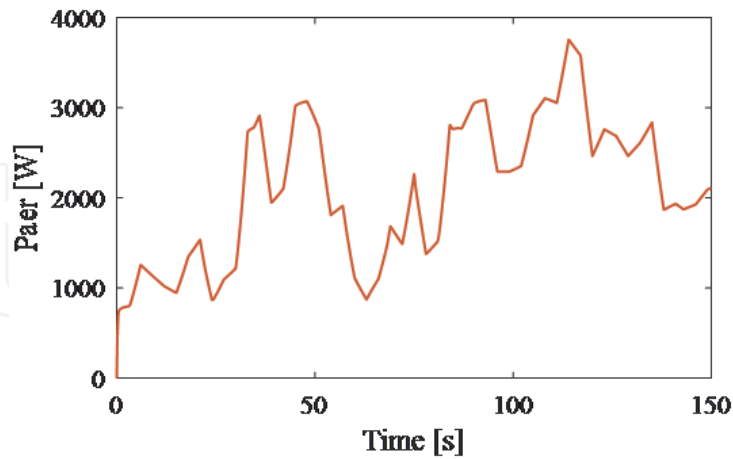


Figure 15.
Aerodynamic power [W].

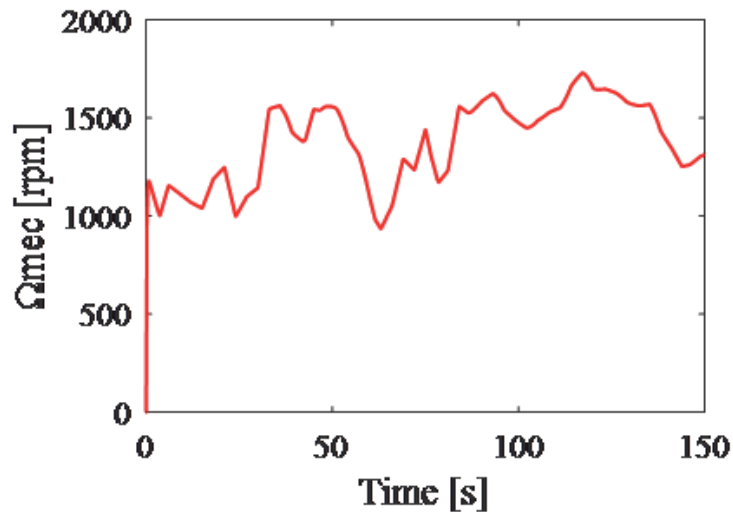


Figure 16.
Mechanical speed of DFIG [rpm].

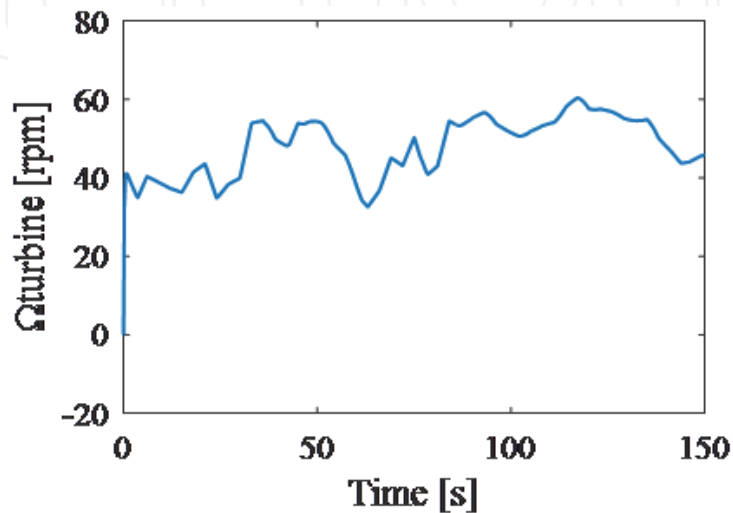


Figure 17.
Turbine speed [rpm].

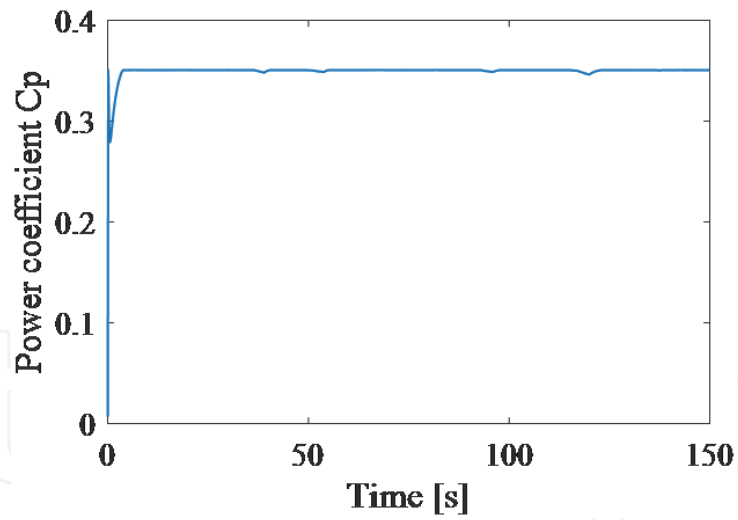


Figure 18.
Power coefficient C_p .

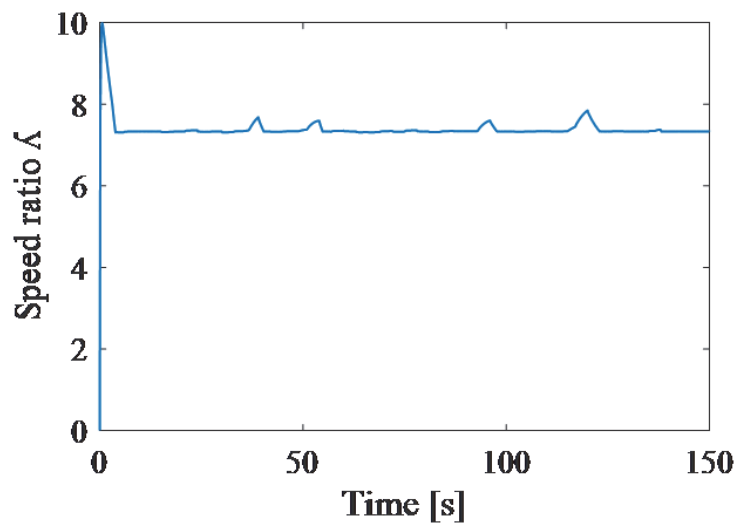


Figure 19.
Speed ratio λ .

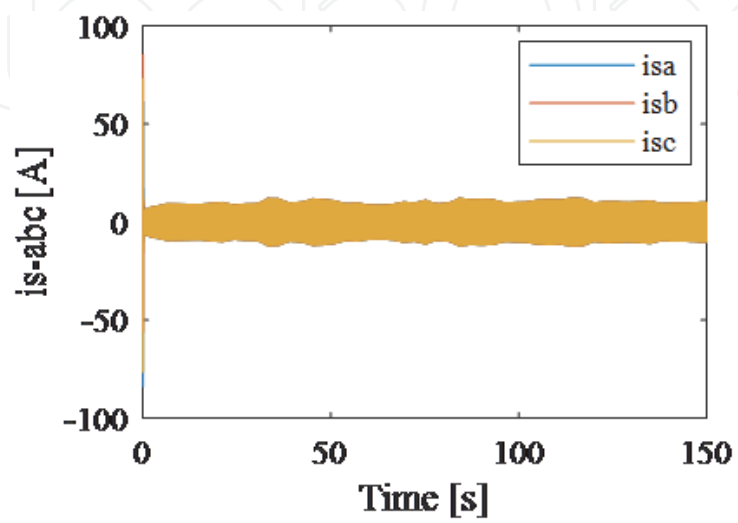


Figure 20.
Three-phase stator current [A].

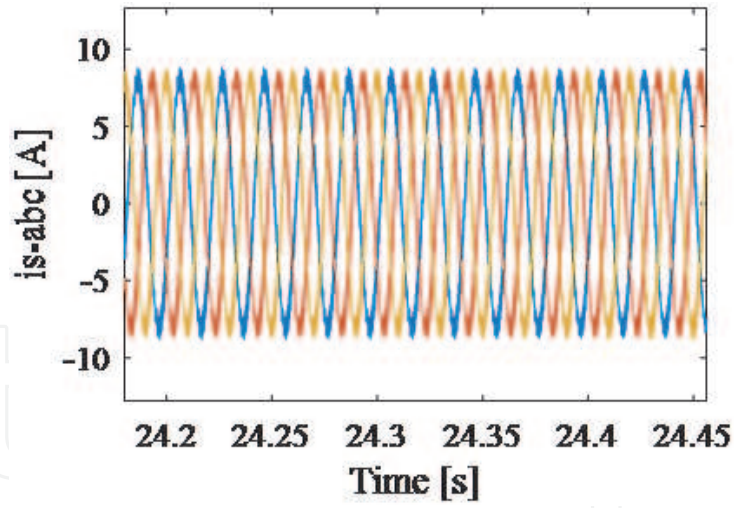


Figure 21.
Zoom on the stator currents [A].

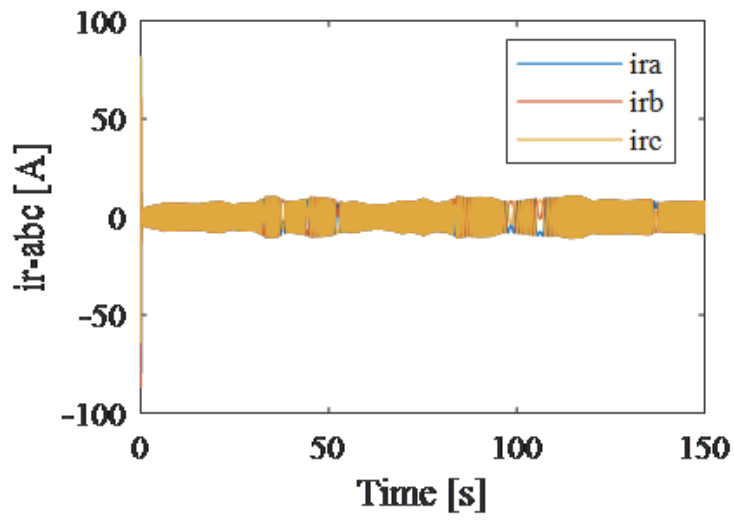


Figure 22.
Three-phase rotor current of DFIG [A].

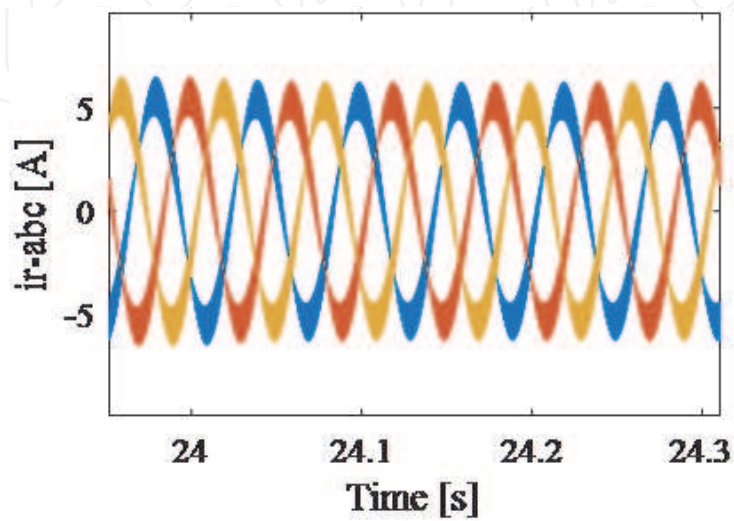


Figure 23.
Zoom on the rotor currents [A].

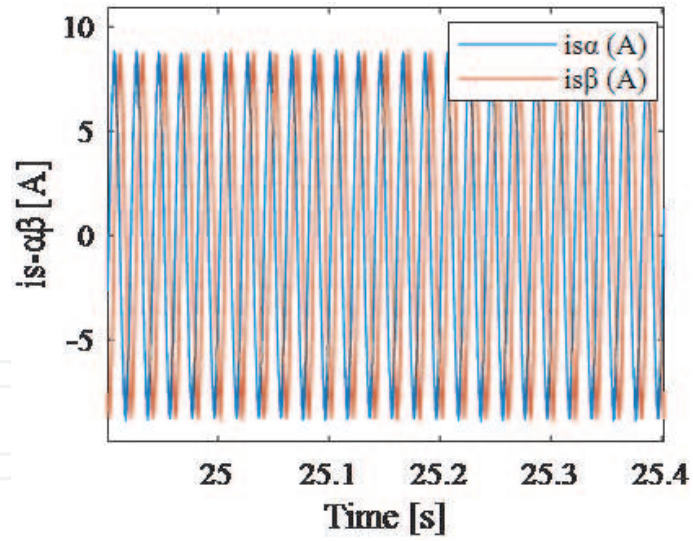


Figure 24.
The stator currents in the (α, β) reference [A].

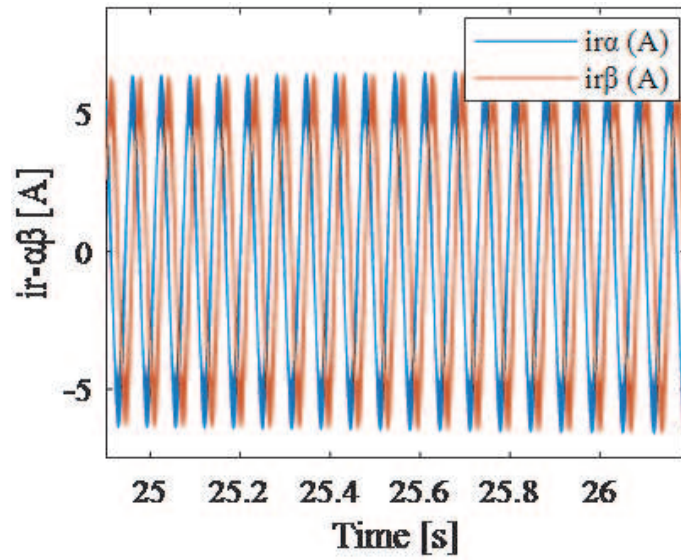


Figure 25.
The rotor currents in the (α, β) reference [A].

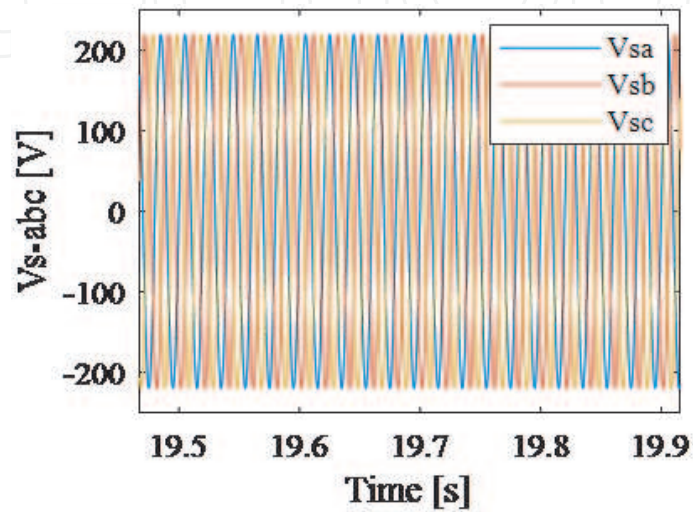


Figure 26.
Three-phase stator voltage [V].

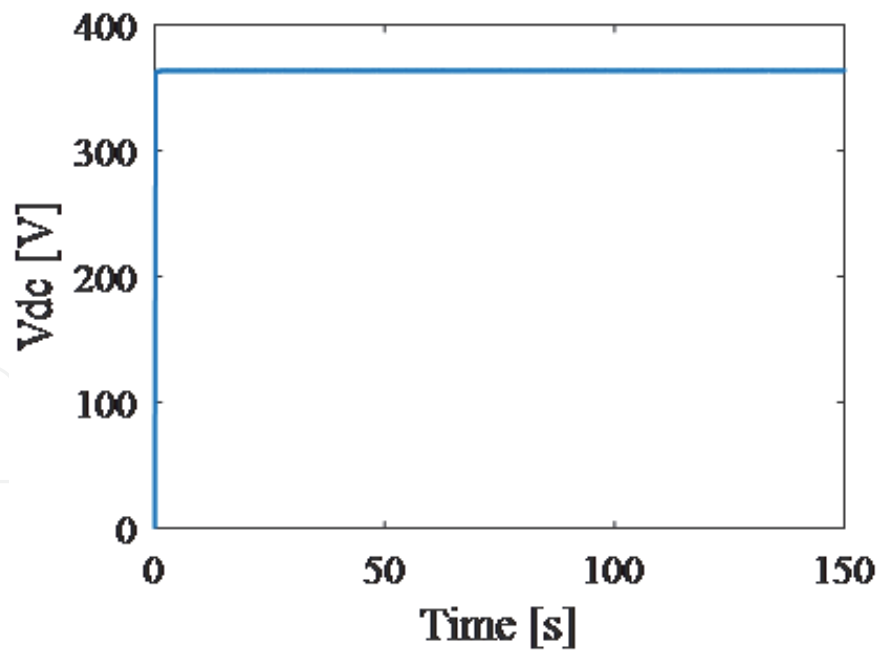


Figure 27.
 Voltage of the DC capacitor [V].

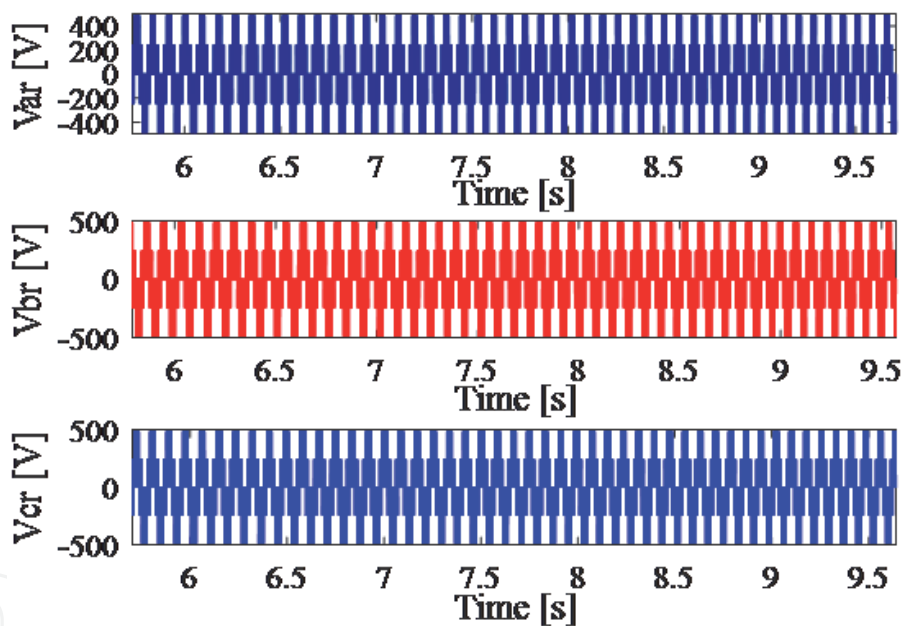


Figure 28.
 The output voltages of the rotor side converter [V].

The wind speed varies between [6 m/s] and [11 m/s]. **Figure 15** presents the aerodynamic power delivered by the wind turbine and it reached 3kw when the wind speed is up to 11 [m/s]. **Figures 16** and **17** illustrate respectively the mechanical speed of the generator shaft and the speed of the turbine shaft. It can be noticed from the **Figure 16** that during the simulation time (150 seconds), the generator operates in both hypo and hyper synchronous operating modes.

The **Figures 18** and **19** show respectively the variation of the power coefficient C_p and the variation of the speed ratio λ , which coincide with the maximum power coefficient and with the optimal speed ratio.

The simulation results of the wind system electrical part, including the electrical characteristics of the DFIG, the power converters, and the capacitive bus, are presented in **Figures 20–27**.

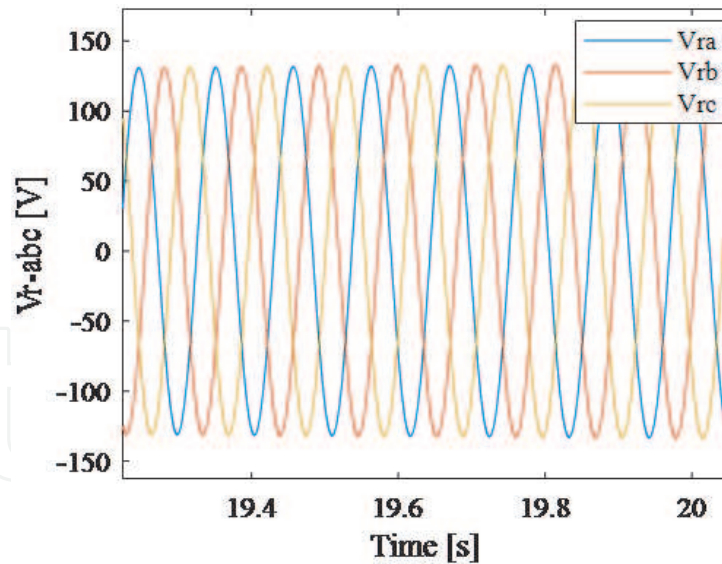


Figure 29.
Three-phase rotor voltage [V].

By applying the first-order passive filter (R, L) to the square-wave signals, given in Figure 28, the rotor voltages in sinusoidal form are obtained and shown in Figure 29.

5. Conclusion

This chapter presents the modeling and simulation results of the most commonly used speed variable wind turbine driven by a doubly fed induction generator. In order to generate efficient and quick electrical power, the control techniques are applied, such as the MPPT control for wind turbine and the stator flux-oriented vector control are used for the generator. The wind turbine system and its control methods are established in the MATLAB/Simulink environment. The obtained signals are used for the design of fault diagnostic methods in future works.

Author details

Imane Idrissi^{1,2*}, Houcine Chafouk², Rachid El Bachtiri³ and Maha Khanfara¹

1 CED: STI, FST, REEPER GROUP, PERE Laboratory, EST, USMBA University, Fez, Morocco

2 IRSEEM, ESIGELEC, Normandy University/UNIRouen, Rouen, France

3 REEPER GROUP, PERE Laboratory, EST, USMBA University, Fez, Morocco

*Address all correspondence to: imane.idrissi@usmba.ac.ma

IntechOpen

© 2019 The Author(s). Licensee IntechOpen. This chapter is distributed under the terms of the Creative Commons Attribution License (<http://creativecommons.org/licenses/by/3.0>), which permits unrestricted use, distribution, and reproduction in any medium, provided the original work is properly cited. 

References

- [1] Global Wind Energy Council, Global Wind Energy Report: Annual Market Update 2017; 2018
- [2] Energy Information Administration. Cost and performance characteristics of new generating technologies. Annual Energy Outlook 2018. 2018. pp. 1-3
- [3] Local Government Association and The Energy Saving Trust. How much do wind turbines cost and where can I get funding? 2009. Available at: http://www.local.gov.uk/home//journal_content/56/10180/3510194/ARTICLE [Accessed: 11 February 2015]
- [4] <http://www.ewea.org/wind-energy-basics/faq/>
- [5] Li H, Chen Z. Overview of different wind generator systems and their comparisons. IET Renewable Power Generation. 2008;2(2):123-138
- [6] Orabi M, El-Sousy F, Godah H, et al. High-performance induction generator-wind turbine connected to utility grid. In: 26th Annual International Telecommunications Energy Conference, INTELEC 2004. IEEE. 2004. pp. 697-704
- [7] Muller S, Deicke M, De Doncker RW. Doubly fed induction generator systems for wind turbines. IEEE Industry Applications Magazine. 2002;8(3):26-33
- [8] Davigny A. Participation aux services système de fermes d'éoliennes à vitesse variable intégrant du stockage inertiel d'énergie [doctoral thesis]. Doctoral School Sciences for the Engineer, University of Sciences and Technology of Lille; 2007
- [9] Belmokhtar K, Doumbia ML, Agbossou K. Modélisation et commande d'un système éolien à base de machine asynchrone à double alimentation pour la fourniture de puissances au réseau électrique. In: Quatrième Conférence Internationale sur le Génie Electrique CIGE. 2010. pp. 03-04
- [10] Burton T, Jenkins N, Sharpe D, et al. Wind Energy Handbook. Chicester, United Kingdom: John Wiley & Sons; 2011
- [11] Kerboua A, Abid M. Hybrid fuzzy sliding mode control of a doubly-fed induction generator speed in wind turbines. Journal of Power Technologies. 2015;95(2):126-133
- [12] Petru T, Thiringer T. Modeling of wind turbines for power system studies. IEEE Transactions on Power Systems. 2002;17(4):1132-1139
- [13] Junyent-Ferré A, Gomis-Bellmunt O, Sumper A, et al. Modeling and control of the doubly fed induction generator wind turbine. Simulation Modeling Practice and Theory. 2010; 18(9):1365-1381
- [14] Luis AS, Wen Y, de Jesus RJ. Modeling and control of wind turbine. Mathematical Problems in Engineering. 2013;2013:1-13
- [15] Prajapat GP, Senroy N, Kar IN. Wind turbine structural modeling consideration for dynamic studies of DFIG based system. IEEE Transactions on Sustainable Energy. 2017;8(4): 1463-1472
- [16] Syahputra R, Soesanti I. Modeling of wind power plant with doubly-fed induction generator. Journal of Electrical Technology. 2017;1(3):126-134
- [17] Widanagama A, Lidula N, Rajapakse AD, Muthumuni D. Implementation, comparison and application of an average simulation model of a wind turbine driven doubly fed induction generator. Energies. 2017; 10(11):1726

- [18] Boukhamkham H. Diagnostique des défaillances dans une machine asynchrone utilisée dans une chaîne éolienne [doctoral thesis]. University of Mohamed Khider Biskra; 2011
- [19] Toual B. Modélisation et commande floue optimisée d'une génératrice à double alimentation, application à un système éolien à vitesse variable [doctoral thesis]. University of Batna 2; 2010
- [20] Azzouz T. Modélisation et commande d'un système de conversion d'énergie éolienne à base d'une MADA [doctoral thesis]. Mohamed Khider-Biskra University; 2015
- [21] Tameghe T, Andy T. Modélisation et simulation d'un système de jumelage éolien-diesel alimentant une charge locale [doctoral thesis]. University of Quebec in Abitibi-Témiscamingue; 2012
- [22] Report ReGrid: Basics of wind energy. Renewables Academy (RENAC) AG, Schönhauser Allee 10-11, 10119 Berlin (Germany)
- [23] Aguglia D, Viarouge P, Wamkeue R, et al. Determination of fault operation dynamical constraints for the design of wind turbine DFIG drives. *Mathematics and Computers in Simulation*. 2010; **81**(2):252-262
- [24] Ackermann T. *Wind Power in Power Systems*. John Wiley & Sons; 2005
- [25] Bechouche A. Utilisation des techniques avancées pour l'observation et la commande d'une machine asynchrone: application à une éolienne [doctoral thesis]. Mouloud Mammeri University; 2013
- [26] Atoui I. Contribution Au Diagnostic De Defauts D'une Generatrice Asynchrone Dans Une Chaîne De Conversion D'énergie Eolienne [doctoral thesis]. Badji Mokhtar University of Annaba; 2015
- [27] Sylla AM. Modélisation d'un émulateur éolien à base de machine asynchrone à double alimentation [doctoral thesis]. University of Quebec at Trois-Rivières; 2013
- [28] El Aimani S. Modélisation des différentes technologies d'éoliennes intégrées dans un réseau de moyenne tension [doctoral thesis]. Central School of Lille; 2004
- [29] Hacil M. Amélioration des performances des énergies éoliennes; 2012
- [30] Pascal K. Modélisation et mise en œuvre d'une chaîne de production éolienne à base de la MADA. Autre. 2013
- [31] Poitiers F. Etude et commande de génératrices asynchrones pour l'utilisation de l'énergie éolienne-machine asynchrone a cage autonome-machine asynchrone à double alimentation reliée au réseau [doctoral thesis]. University of Nantes; 2003
- [32] Bossoufi B, Karim M, Lagrioui A, et al. Observer backstepping control of DFIG-generators for wind turbines variable-speed: FPGA-based implementation. *Renewable Energy*. 2015;**81**:903-917
- [33] Idrissi I, Chafouk H, et al. A bank of Kalman filters for current sensors faults detection and isolation of DFIG for wind turbine. In: 2017 International Renewable and Sustainable Energy Conference (IRSEC). IEEE. 2017. pp. 1-6
- [34] Shao S, Abdi E, Barati F, et al. Stator-flux-oriented vector control for brushless doubly fed induction generator. *IEEE Transactions on Industrial Electronics*. 2009;**56**(10): 4220-4228